# Nanoscale Plasmonic Stamp Lithography on Silicon

Fenglin Liu,[†,‡] Erik J. Luber,[†,‡] Lawrence A. Huck,[†,‡,§] Brian C. Olsen,[†,‡] and Jillian M. Buriak*[,†,‡]

[†]Department of Chemistry, University of Alberta, 11227 Saskatchewan Drive, Edmonton, AB T6G 2G2, Canada and [‡]National Institute for Nanotechnology, National Research Council Canada, 11421 Saskatchewan Drive, Edmonton, AB T6G 2M9, Canada. [§]Present address: (L.A.H.) Gilead Alberta ULC, 1021 Hayter Road Edmonton, Alberta T6S 1A1, Canada.

ABSTRACT Nanoscale lithography on silicon is of interest for applications ranging from computer chip design to tissue interfacing. Block copolymer-based self-assembly, also called directed self-assembly (DSA) within the semiconductor industry, can produce a variety of complex nanopatterns on silicon, but these polymeric films typically require transformation into functional materials. Here we demonstrate how gold nanopatterns, produced *via* block copolymer self-assembly, can be incorporated into an optically transparent

flexible PDMS stamp, termed a plasmonic stamp, and used to directly functionalize silicon surfaces on a sub-100 nm scale. We propose that the high intensity electric fields that result from the localized surface plasmons of the gold nanoparticles in the plasmonic stamps upon illumination with low intensity green light, lead to generation of electron—hole pairs in the silicon that drive spatially localized hydrosilylation. This approach demonstrates how localized surface plasmons can be used to enable functionalization of technologically relevant surfaces with nanoscale control.
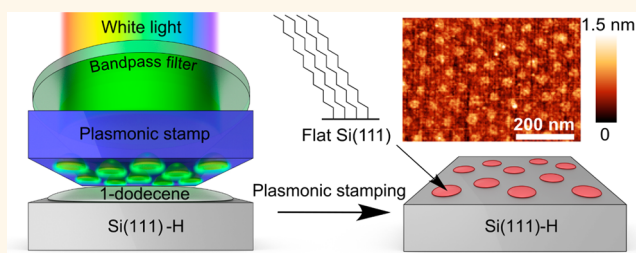
KEYWORDS: block copolymer · nanolithography · self-assembly · localized surface plasmon · hydrosilylation · nanopattern · silicon · surface

N anopatterned surfaces are of central importance to a variety of areas and applications,[1] such as computer chip architectures,[2,3] tissue interfacing,[4,5] biosensors,[6] light management and plasmonics,[7] among others. Typically, the various approaches to nanopatterning are broken into two major classes: top-down methods such as photolithography, e-beam lithography, and scanning force microscopy variants,[8–11] and bottom-up synthetic techniques, including self-assembly.[12–14] Since lithography is the single most expensive step in computer chip manufacturing, the use of self-assembled block copolymers (BCPs) templates on surfaces is being seriously considered by the semiconductor industry to pattern sub-20 nm features on a semiconductor surface; the Industry Technology Roadmap for Semiconductors (ITRS) terms this development "directed self-assembly", or DSA.[15] Thanks to the enormous amount of work devoted to BCP-based lithography over the past two decades,[16–19] there is a plethora of patterns and morphologies that can be obtained, ranging from self-assembled BCP-derived nanostructures such as hexagonally packed dots,[20,21] lamellae,[22,23] and cylinders[24–27] to the highly complex and long-range ordered bends,[13] triangles,[28] and junctions[29,30] produced *via* directed self-assembly.

BCP-based films are compatible with existing silicon-based lithography[31,32] due to the central role played by organic photoresists that are handled in much the same manner. As is the case with photoresists, the nanostructured BCP films must typically still be translated or converted into a functional material or used directly as a removable etch stop.[33] For instance, metal nanopatterns can be converted by loading polystyrene-*block*-polyvinylpyridine films with metal ions and then treated with plasma to remove the BCP and simultaneously reduce the metal ions to metal nanostructures.[34,35] Complex nanopatterned silica structures can be obtained directly *via* plasma treatment of annealed polystyrene-*block*-polydimethylsiloxane (PS-*b*-PDMS) BCP films.[36] BCP films can also act as a nanostructured etch stop to yield three-dimensional nanostructures in the underlying silicon,[37,38] GaAs,[39] and other substrates.[40]
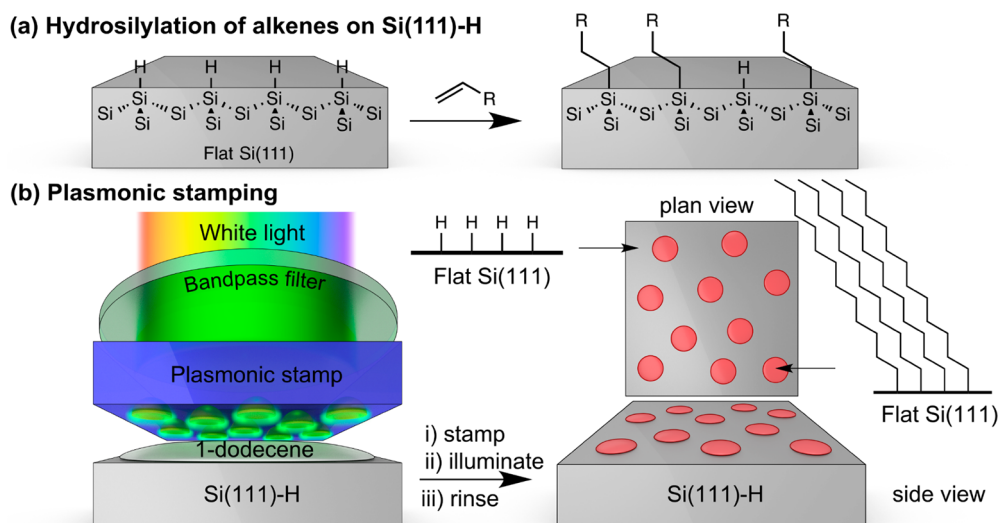
Figure 1. Scheme of hydrosilylation reaction on silicon surface. (a) Hydrosilylation of an alkene on Si(111)−H, resulting in Si−C bond formation and covalent attachment of the molecule to the surface. (b) Schematic outline of plasmonic stamp-assisted photohydrosilylation on a Si(111)−H surface. A continuous wave bandpass filter, where it shines upon the optically transparent, PDMS-based plasmonic stamp with embedded gold nanoparticle patterns. Hydrosilylation occurs in a spatially defined fashion on the Si(111)−H surface to produce a hydrosilylated surface pattern that mirrors that of the parent gold nanoparticle pattern in the plasmonic stamp.

The nanopatterning of molecules on a surface using BCPs to direct reactivity is much more challenging and has been the subject of far less attention. BCPs have been applied to enable molecular transfer printing by Nealey and co-workers[41] and have been used to direct the reactivity of diazonium salts on carbon surfaces,[42] but the area remains relatively unexplored.

In this work, we show how gold nanopatterns formed *via* BCP self-assembly can be incorporated into an optically transparent flexible stamp made up of polydimethylsiloxane (PDMS) and then used to drive molecular reactions on a silicon surface in a spatially defined manner. The approach is based upon the localized surface plasmon resonance (LSPR) of the gold nanoparticles, driving a hydrosilylation reaction on Si(111)−H surfaces, as shown in Figure 1. The generation of high intensity local electric fields by a LSPR is well established (up to 10^3-fold enhancement)[43,44] and has been applied to a variety of materials-based applications such as surface-enhanced Raman scattering (SERS), photocatalytic water splitting,[45] and photovoltaics.[46,47] With respect to hydrosilylation, the Sugimura group[48] showed that gold nanoparticles capped with alkene-terminated thiols showed higher levels of incorporation on Si(111)−H when illuminated with light that overlapped with the absorption maximum of the gold nanoparticles. The authors referred to the gold nanoparticles as "photon collectors",[48] transferring the energy of the incident illumination to the surface; while a tantalizing result, the mechanism remains largely unexplored.

The chemical reaction that is the focus of this work, hydrosilylation, involves the insertion of an unsaturated bond, in this case an alkene, into a silicon−hydride group on the surface, which results in attachment of the alkyl to the silicon *via* a Si−C bond.[49−53] This reaction is of broad interest because of its utility for covalent interfacing of a broad range of organic molecules to silicon surfaces.[52,54−56] The reaction pathways proposed for low energy light-induced hydrosilylation reactions on the silicon surface typically involve electron−hole pairs, since visible light is incapable of homolytic Si−H bond cleavage or electron photoemission.[57] We will provide mechanistic insights that strongly point toward the role of the LSPR of a proximal gold nanoparticle dramatically increasing the efficiency of electron−hole pair generation at the silicon surface, leading to efficient surface-localized hydrosilylation. Through the use of spatially defined gold nanoparticle patterns within the plasmonic stamps employed, the organic functionalization can be patterned with sub-100 nm resolution.
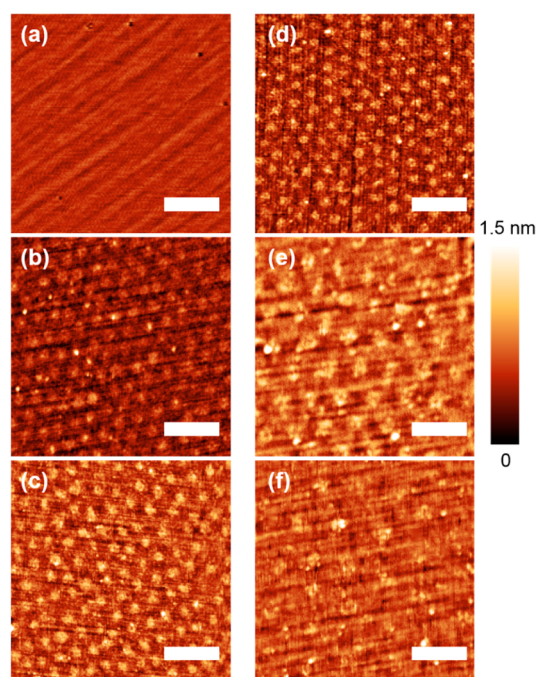
RESULTS AND DISCUSSION

The fabrication of optically transparent PDMS-based plasmonic stamps was carried out in a manner similar to the approach used to synthesize Pd− and Pt−nanoparticle catalytic stamps, as previously described.[58−60] Briefly, hexagonal nanopatterns of gold hemispheres on silicon were prepared by BCP self-assembly. In the example shown in Figures 2a,b and in Figure S1 (Supporting Information), the BCP chosen was PS-*b*-P2VP, with a molecular weight of 125 k-*b*-58.5 k, which upon self-assembly and annealing yielded a hexagonal pattern of micelles with a center-to-center spacing of 70 nm. The self-assembled BCP template was loaded with KAuCl$_4$ and converted into gold nanopatterns upon plasma

(a) Fabrication of plasmonic stamp

(b-e) Characterization of plasmonic stamp
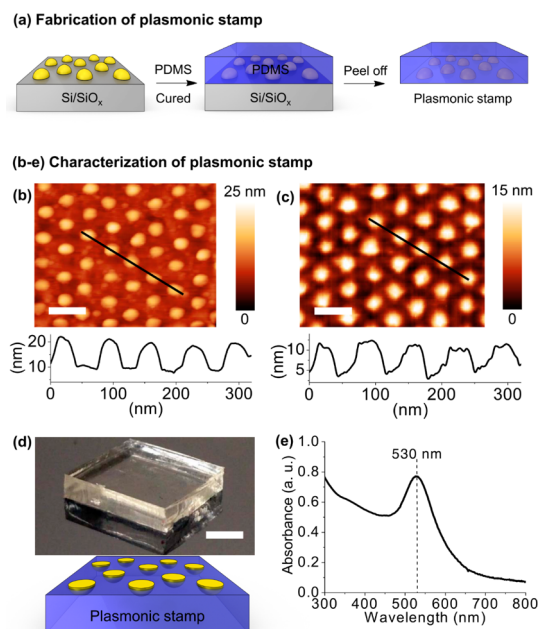
Figure 2. Fabrication and characterization of plasmonic stamps. (a) Conversion of a gold nanopattern on silicon, prepared *via* block copolymer self-assembly, into a plasmonic stamp. A gold nanopattern is produced using a self-assembled block copolymer (BCP) template and then lifted off the Si/SiO$_x$ surface embedded within the cured PDMS to yield the plasmonic stamp. (b) Atomic force microscopy (AFM) height map and section analysis of a gold nanopattern on silicon surface, produced *via* self-assembly of the BCP PS-*b*-P2VP (molecular weight of 125 k-*b*-58.5 k). The scale bar is 100 nm. (c) AFM height map and section analysis of the plasmonic stamp surface. The scale bar is 100 nm. (d) Schematic image and optical photograph of a plasmonic stamp (on a reflective surface). The scale bar is 2 mm. (e) UV−vis spectrum of a PDMS plasmonic stamp showing the absorption at 530 nm due to the embedded gold nanoparticles.


Figure 3. AFM height maps of silicon surfaces with 1-dodecene and plasmonic stamps. (a−c) Effect of time on illumination of a Si(111)−H surface with 1-dodecene, through a plasmonic stamp, from 0 (a), 30 (b), and 60 min (c). The parent BCP used for the gold nanoparticle pattern embedded within the plasmonic stamp was PS-*b*-P2VP (molecular weight of 125 k-*b*-58.5 k). (d−f) Control over pattern spacing using plasmonic stamps prepared with BCPs of 3 different molecular weights: center-to-center spacings of PS-*b*-P2VP (125 k-*b*-58.5 k) and illumination time of 60 min was 70 nm (d), PS-*b*-P2VP (91.5 k-*b*-105 k) was 120 nm (e), and PS-*b*-P2VP (190 k-*b*-190 k) was 160 nm (f). All scale bars correspond to 200 nm.

treatment, which simultaneously reduced the Au(III) salt to Au(0) and removed the BCP.[20,21] The gold nanopatterns on silicon were then coated with PDMS precursors and allowed to cure. When the plasmonic stamp was peeled off the silicon, the gold hemispheres remained embedded within the plasmonic stamp, with the flat faces of the gold hemispheres exposed on one side of the plasmonic stamp, as shown in Figures 2c,d. In the example here, the plasmonic stamps were 1.0 × 1.0 cm^2, ∼4 mm thick, and show an absorbance peak at 530 nm in the UV−vis spectrum, which is attributed to the LSPR of the gold nanoparticles (Figure 2e).

The LSPR-assisted hydrosilylation was carried out by applying the gold-nanopatterned plasmonic stamp on a hydride-terminated silicon (111) surface, referred to as Si(111)−H, prepared *via* 4 min etch in 40% NH$_4$F (aq). Neat 1-dodecene (30 μL) was then dropped onto the Si(111)−H surface in a nitrogen-filled glovebox and the plasmonic stamp placed on top in direct contact; this PDMS/1-dodecene/Si(111)−H sandwich was then firmly clamped together, as shown in Figure 1b (photograph in Figure S2, Supporting Information). The surface of the silicon was then illuminated through

the plasmonic stamp with green light of mild intensity (50 mW/cm^2); filter: CW526 (center band wavelength: 526 nm); fwhm (full width-half max: 180 nm) for the desired period of time (0 to 60 min); the silicon sample was then released, rinsed with dichloromethane, dried under an argon stream, and then analyzed by atomic force microscopy (AFM). An AFM micrograph of a freshly etched Si(111)−H surface shows the expected Si(111) terrace planes (Figure 3a). The hexagonal pattern of dodecyl spots on the Si(111) starts to emerge after 30 min of illumination (Figure 3b) and becomes more apparent after 60 min (Figure 3c). The center-to-center spacing of the hexagonal spots can be controlled by varying the molecular weight of the BCPs; Parts d−f of Figure 3 show dodecyl patterns with the expected heights for dodecyl chains (∼1.0 nm, Figure S3, Supporting Information), with center-to-center spacings of 70, 120, and 160 nm, prepared with PS-*b*-P2VP BCPs of molecular weights of 125 k-*b*-58.5 k, 91 k-*b*-105 k, and 190 k-*b*-190 k, respectively. The resulting patterns show good fidelity with respect to the parent gold nanoparticle patterns. In order to verify that these patterns are a result of localized hydrosilylation, further chemical functionalization was carried out,
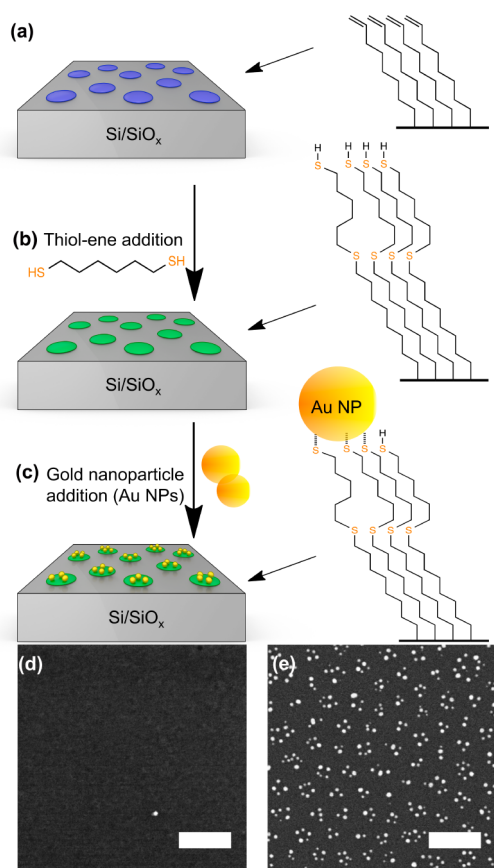
Figure 4. Pattern modification/visualization using 10 nm gold nanoparticles. (a–c) Schematic outline of pattern visualization *via* multiple surface modification reactions. The BCP used for generating the gold nanoparticle pattern within the plasmonic stamp was PS-*b*-P2VP (molecular weight is 125 k-*b*-58.5 k). Hydrosilylation with 1,7-octadiene resulted in alkene-terminated patterns; a UV-mediated thiol−ene addition of 1,6-hexanedithiol resulted in thiol-terminated patches. Exposure of this patterned surface to gold nanoparticles resulted in binding only to the thiol-terminated areas on the silicon surface. (d) Scanning electron microscopy (SEM) micrograph of the patterned silicon surface before exposure to gold nanoparticles. (e) SEM micrograph of patterned silicon surface after exposure to ∼10 nm Au nanoparticles. (SEM scale bar: 100 nm).

with the goal of binding gold nanoparticle tags to the spots in the hexagonal patterns for SEM imaging. A bis-diene was used as the ink for stamp-mediated hydrosilylation, since hydrosilylation of this molecule would yield ω-alkenyl-terminated spots, with center-to-center spacings of 70 nm (Figure 4). Thiol−ene click chemistry on the ω-alkene groups with a dithiol would be expected to lead to spots with terminal thiol groups;[61,62] exposure of the functionalized silicon to citrate-capped ∼10 nm-diameter gold nanoparticles resulted in binding of the nanoparticles to the thiol-capped spots, giving rise to a templated hexagonal nanopattern, as shown in Figure 4.

A series of control experiments support the proposal that the gold nanoparticles are essential to enable light-induced hydrosilylation. Illumination of a blank plasmonic stamp (missing gold nanoparticles), or
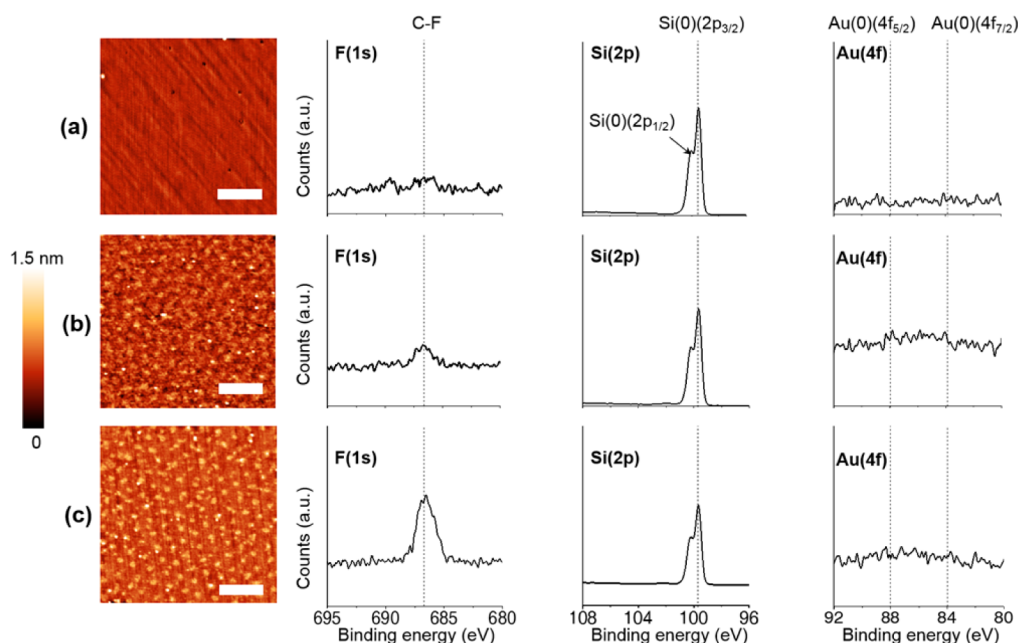
applying the gold-nanopatterned plasmonic stamp in the dark, revealed no dodecyl patterns on the surface, as summarized in Figure 5, Figure S4, and Table S1 (Supporting Information). To provide further evidence, a fluorinated alkene, 1*H*,1*H*,2*H*-perfluoro-1-decene, was tested for LSPR-mediated hydrosilylation, using the same conditions as those described earlier for 1-dodecene, which was characterized *via* X-ray photoelectron spectroscopy (XPS) and contact angle (goniometry) measurements. The AFM images and corresponding XPS data for nanopatterned Si(111)−H at 0, 30, and 60 min of illumination are shown in Figure 6; as can be seen from the XPS data, the F(1*s*) signal (687.3 eV) increases in intensity with increased time, and the high-resolution spectra of the Au(4*f*) and Si(2*p*) regions show the absence of features that would correspond to residual gold (84 and 88 eV),[63] PDMS (∼102 eV),[64] and oxidized surface-bound silicon (∼103 eV).[64] The corresponding contact angle measurements for these surfaces are shown in Figure 5 and Table S1 (Supporting Information). The contact angle of the Si(111)−H surface was found to measurably increase only when the surface was subjected to the combination of both a plasmonic stamp and illumination. The maximum observed contact angles for patterned Si(111)−H surfaces were 98° and 105° for hydrosilylation with 1-dodecene, and 1*H*,1*H*,2*H*-perfluoro-1-decene, respectively.

As determined by UV−vis spectroscopy, the absorbance maximum of the LSPR stamp was observed at 530 nm (Figure 2e). To determine if the plasmon resonance was fundamental to the observed hydrosilylation, samples were illuminated with light having no spectral overlap with the plasmon resonance of the gold nanoparticles. To this end, the same light source was used, but with a band-pass filter (CW 440 nm) centered around 440 nm fwhm of 90 nm, which allows passage of higher energy light, but cuts off just below the absorbance of the plasmon. This experiment resulted in no obvious pattern transfer *via* hydrosilylation on the Si(111)−H surface, as demonstrated by contact angle measurements (Figure 5 and Table S1, Supporting Information) and AFM characterization (Figure S5, Supporting Information).

From the above results, it appears that the local hydrosilylation reaction is driven by the plasmon resonance of the Au nanoparticles. As such, energy is being transferred from the Au nanoparticles/plasmons to the 1-dodoecene/Si(111)−H interface. Upon excitation, the plasmon can decay radiatively through resonant photon scattering or nonradiatively *via* the generation of an electron−hole pair (EHP), typically referred to as hot carriers.[43,65] These hot carriers can be directly injected into the surrounding medium, or they can recombine, which results in local heating of the nanoparticle. Lastly, EHPs can be directly generated in the Si as a result of the high intensity electromagnetic
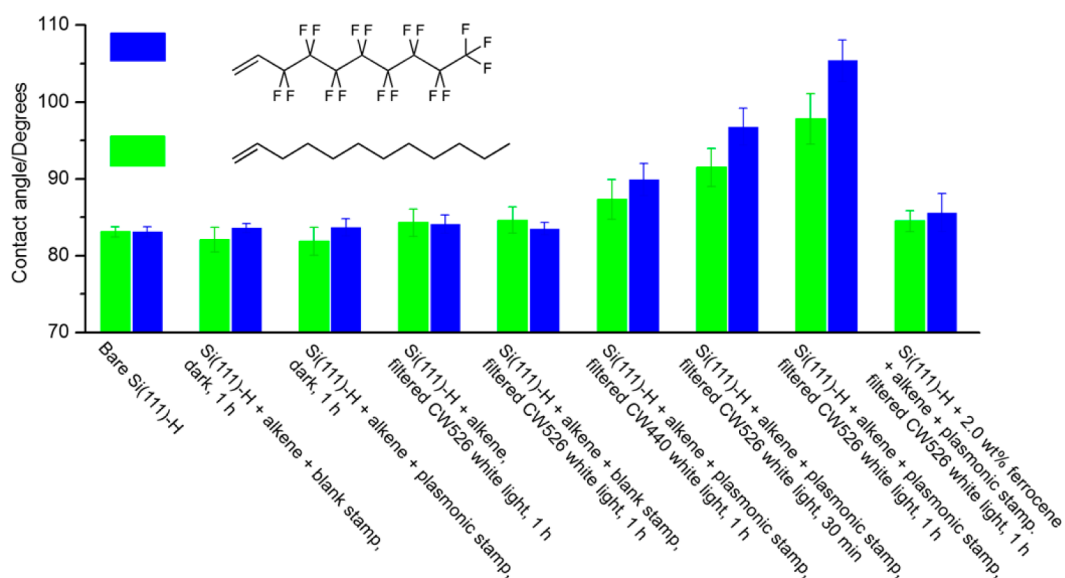
Figure 5. Contact angle measurements. Comparison of contact angles of Si(111)—H surfaces following hydrosilylation of 1-dodecene (black) and 1*H*,1*H*,2*H*-perfluoro-1-decene (blue), under various conditions, many of which are considered to be control experiments. The detailed summary of contact angle measurements and corresponding statistics/errors are listed in Table S1 and Figures S7 and S8, Supporting Information.

Figure 6. AFM height maps and corresponding high-resolution XPS spectra of the hydrosilylation of 1*H*,1*H*,2*H*-perfluoro-1-decene on Si(111)—H through a plasmonic stamp with different illumination times. The parent BCP for the gold nanopattern is PS-*b*-P2VP (125 k-*b*-58.5 k) (a) without illumination for 60 min, (b) 30 min illumination, and (c) 60 min illumination. High-resolution X-ray photoelectron spectroscopy (XPS) of each sample was taken of the F(1*s*), Si(2*p*), and Au(4*f*) regions (AFM scale bar: 200 nm).

field of the LSPR, which is localized to the neighborhood of the gold nanoparticle. Given that all four of these mechanisms (resonant photon scattering, nanoparticle plasmonic heating, hot carrier injection and near-field electromagnetic EHP generation) could be driving the local hydrosilylation reaction, their relative contributions are discussed below.

Efficiency enhancement due to the resonant photon scattering or forward light scattering of metal

nanoparticles has been suggested in the field of light scattering-enhanced solar cells.[47,66] When metal nanoparticles are located on a solar cell surface, the secondary radiation of incident electromagnetic energy scattered into the active layers of solar cells, referred to as the forward light scattering, can increase the effective optical length by light trapping in the active layers which could lead to an increased rate of EHP generation at the silicon surfaces. However, the size of the Au

nanoparticles in the plasmonic stamp is 10−15 nm, which is in the range in which LSPR absorption would be dominant; the forward scattering intensity would be less than 0.1% of incident light, according to previously reported simulations.[66,67]

The next mechanism to be considered is in situ plasmonic heating, which could result in a local increase of temperature of the gold nanoparticles due to the strong light absorption at the plasmon resonance, which is dissipated as heat.[68,69] For thermal heating to play a role in hydrosilylation, the silicon surface would need to reach temperatures in excess of 100 °C, within the time scale of experiments performed in this work.[70] The temperature increase, ΔT, of a single isolated gold nanoparticle can be estimated using the conventional model[71]

$$\Delta T = \frac{\sigma I}{2\pi k D}$$

where σ is the particle absorption cross section, I is the incident light intensity, k is the thermal conductivity of the surrounding medium, and D is the nanoparticle diameter. Assuming a scattering cross section of 500 nm^2, a thermal conductivity of 0.15 W/m K (corresponding to PDMS), a nanoparticle diameter of 15 nm, and an intensity of 50 mW/cm^2, the predicted temperature increase would be 1.8×10^{-5} °C. It is worth noting that steam generation has been observed for dilute solutions of light absorbing nanoparticle using moderate light intensities of $\sim 10^5$ mW/cm^2,[68] but this phenomenon has been shown to be a result of enhanced light absorption due to efficient volume scattering between nanoparticles in solution.[72] A similar light trapping effect is unlikely to play a role here since the nanoparticles are isolated on a single plane. Moreover, in order for patterned surface hydrosilylation to occur, it would be necessary for the temperature increase to be localized directly underneath the nanoparticles such that the surrounding silicon does not react. This effect has been extensively studied by Baffou et al.,[73] who showed that localized heating around the nanoparticles could only take place if they were sufficiently far apart relative to the total number of illuminated nanoparticles, due to heat diffusion between nanoparticles. Specifically, it was shown through both simulation and experiment that localized heating could only be achieved if $p^2/3LR \gg 1$, where p is the average center-to-center spacing, R is the nanoparticle radius, and L is the diameter of the illuminated area. Given that $p^2/R \sim 650$ nm, while the illuminated diameter is on the order of millimeters, it can be concluded that any temperature increase due to nanoparticle heating would be uniformly distributed across the substrate surface. Lastly, at the macroscale, illumination of the plasmonic stamp/1-dodecene/Si(111)−H sandwich with filtered white light (50 mW/cm^2, CW526), resulted in only a minor

temperature change from room temperature to a maximum temperature ~ 35 °C, in about 20−30 min, as measured with a small thermocouple localized between the plasmonic stamp and silicon (see Figure S6, Supporting Information).

The third mechanism to consider is hot carrier injection from the gold nanoparticles into the surrounding medium. In the event of nonradiative decay of the plasmon (which is the dominant plasmon decay mode for nanoparticles much smaller than the plasmon wavelength),[74] an energetic EHP is formed, typically referred to as hot carrier generation. These hot carriers have been extensively studied in catalytic water-splitting, where it has been shown that the hot carriers are directly injected into the semiconductor surface, facilitating the water-splitting reaction.[75,76] In the case of hydrosilylation, if a hole is injected into the silicon surface from the gold nanoparticle, the hydrosilylation reaction can proceed via nucleophilic attack by an alkene on a positively charged surface silicon site, as has been repeatedly postulated.[51,77] However, it is necessary to consider the presence of the nonconducting organic layer of 1-dodecene sandwiched between the gold nanoparticles and the silicon surface, which would be expected to impede charge transfer to the silicon. Although the 1-dodecene is layer is nonconducting, recent work has revealed that the plasmonically generated hot holes in gold can have energies of ~ 7.5 eV (relative to vacuum),[78] and as such it is possible that some of these hot holes could be injected into the silicon. These injected holes could then lead to hydrosilylation via nucleophilic alkene attack and silicon−carbon bond formation.[51] Although direct charge transfer of hot carriers from the gold nanoparticle to the silicon surface appears to be unlikely in this scenario, further investigation is necessary to conclusively determine the role of these hot carriers.

Lastly, the effect of the highly concentrated electromagnetic field produced by the LSPR is considered. It has been shown that the rate of EHP generation in a semiconductor is proportional to the local intensity of the electric field.[79,80] Given that the electric field enhancement is on the order of $\sim 10^3$ at the edges of the nanoparticle,[43] the relative concentration of EHPs at the silicon surface (within the neighborhood of the gold nanoparticle) would also be expected to $\sim 10^3$ times higher. As such, the kinetic rate of the hydrosilylation reaction would proceed much faster in these areas of increased EHP concentration, given that the EHPs drive the reaction, as outlined in Scheme 1.

To support a hydrosilylation mechanism of plasmon-induced reactive carriers in the silicon, trace amounts of a charge-transfer quenching agent, ferrocene, were added to the 1-dodecene; if such a mechanism were to be in play, the ferrocene should effectively quench the reaction via electron injection because the holes required to drive the hydrosilylation mechanism would

Scheme 1. Proposed Mechanism for the Plasmonic Stamp-Assisted Hydrosilylation[a]
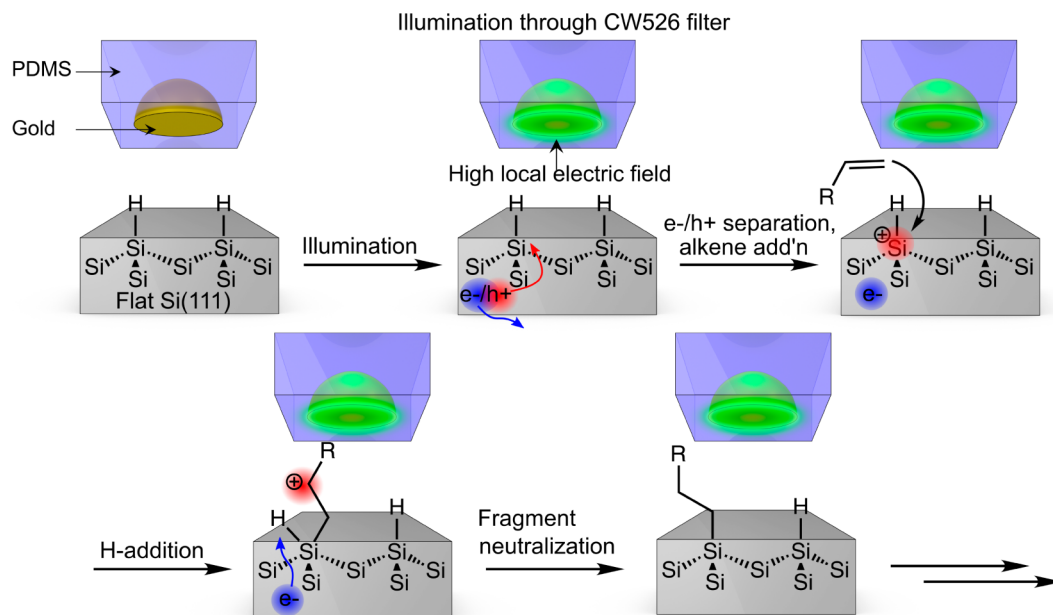
[a]Upon illumination of filtered light (CW526, 50 mW/cm^2, green color), the induced localized surface plasmon resonance (LSPR) of a gold nanoparticle embedded within the PDMS-based plasmonic stamp results in an enhanced local electric field ("green glow"). The local electric field results in an enhanced rate of proximal formation of electron-hole pairs on the silicon surface. Holes at the Si(111)−H interface are then attacked in a nucleophilic fashion to generate a Si−C bond;[53,77] as has been previously surmised, the resulting β-silyl-substituted carbocation is stabilized by hyperconjugation, and the alkyl chain is rendered neutral with a combination of a local H and an electron.[50]

be eliminated in situ.[57,77] Addition of 2.0% ferrocene (w/w) to the 1-dodecene resulted in no visible pattern by AFM and an unchanged contact angle (Figure 5), suggesting ex situ hole quenching *via* electron transfer from the ferrocene, providing an addition piece of evidence to substantiate the mechanism based upon electron/holes (Scheme 1).

CONCLUSION

Localized surface plasmons in a gold nanopattern, embedded within an optically transparent plasmonic stamp, can be used to drive hydrosilylation of alkenes on silicon surfaces, upon illumination with low intensity light with wavelengths that corresponded to the absorption profile of the gold nanoparticles. The gold nanopatterns were created *via* block copolymer self-assembly, but could presumably be produced through other lithographic nanopatterning approaches. The most likely mechanism for the observed hydrosilylation is based upon the high intensity local electric field of the gold nanoparticle LSPRs leading to the generation of electron−hole pairs in the silicon, resulting in nucleophilic attack by the alkene, and formation of the Si−C bond. The resulting patterns on the silicon surface mirror those of the parent gold nanopattern within the plasmonic stamp, and demonstrate the localized nature of the reaction. Other surface reactions that are driven by locally generated charges may also be promoted by the plasmonic stamp, and the influence of hot-spots, edges, points, and other features that result in increased electric field effects could provide a rich source of reactivity.

EXPERIMENTAL SECTION

Materials. All reagents and materials were used as received unless otherwise specified. Si wafers (111 plane-oriented, prime grade, p-type, B-doped, ρ = 1−10 Ω-cm, thickness = 600−650 μm) were purchased from WRS Materials, Inc. Millipore water (resistivity: 18.2 MΩ·cm) was used for the preparation of all aqueous solutions and for rinsing samples. Block copolymers (BCPs), all of the composition polystyrene-*block*-poly-2-vinylpyridine (PS-*b*-P2VP) with three different molecular weights (125 k-*b*-58.5 k, 91.5 k-*b*-105 k, and 190 k-*b*-190 k), were purchased from Polymer Source, Inc. The starting materials for preparing *h*-PDMS (VDT-731, HMS-301, and SIP6831.2) were purchased

from Gelest Corp., and 184 PDMS from Dow Corning. 2,4,6,8-Tetramethyl-2,4,6,8-tetravinylcyclotetrasiloxane, 30% NH$_4$OH (aq), 30% H$_2$O$_2$ (aq), KAuCl$_4$·xH$_2$O (99.999%), 1,4-butanedithiol (>97%), trichloro(1H,1H,2H,2H-perfluorooctyl)silane (98%), 1,7-octadiene (>99.0%), 1-dodecene (>99.0%), and 1H,1H,2H-perfluoro-1-decene (99.0%) were obtained from Sigma-Aldrich. 1-Dodecene, 1,7-octadiene, and 1H,1H,2H-perfluoro-1-decene were passed through a column of dried alumina to remove peroxides and deoxygenated with a stream of nitrogen gas. Optical filters (CW526 or CW440, CW referring to center wavelength) were purchased from Edmund Optics, Inc.

Characterization. Atomic force microscopy (AFM) height images in tapping mode were captured using a Digital

Instruments/Vecco Nanoscope IV with silicon PPP-NCHR cantilevers (Nanosensors). Scanning electron microscopy (SEM) images were obtained from a field emission scanning electron microscope (S4800, Hitachi), the working pressure for SEM imaging was $<10^{-8}$ Torr. X-ray photoelectron spectroscopy (XPS) spectra were recorded using an X-ray photoelectron spectrometer (Kratos Axis 165). The binding energies were calibrated using the C(1s) feature at 285.0 eV. Sessile drop contact angle measurements were measured on a contact-angle goniometer (Model 100-00, Rame-Hart) using a 5 μL water droplet. Contact angles are recorded after the droplet reached the equilibrium state on the sample surface.

Silicon Wafer Preparation. Si(111) wafers were cut into 1 × 1 cm^2 pieces, sonicated in methanol for 15 min, and dried with a stream of nitrogen gas. The silicon wafers were then cleaned *via* a standard RCA procedure:[28] The wafers were first immersed in a solution of 30% NH_4OH (aq), water, and 30% H_2O_2 (aq), with volume ratio of 1:6:1 at 80 °C for 15 min, rinsed with water, and then immersed in a solution of 37.5% HCl (aq), water, and 30% H_2O_2 (aq), with volume ratio of 1:5:1 at 80 °C for another 15 min. Lastly, the wafers were rinsed with water and dried with a stream of nitrogen gas.

Preparation of Au Nanopatterns on Si/SiO$_x$ Surface. The BCP solution of PS-*b*-P2VP (125 k-*b*-58.5 k, 1.0 wt % in toluene) was spin-cast at 4000 rpm for 40 s on a clean, native oxide-capped Si(111) wafer and annealed in a home-built annealing chamber, as described previously,[25] which contained 1.0 mL of THF for 60 min; a photograph of the chamber (Figure S9) and additional experimental details are provided in the Supporting Information. The BCP layer on the Si(111) surface was then converted to the corresponding gold nanopattern using a process previously described,[21] with slight modifications: Briefly, the sample was immersed in 10 mL of a 10 mM KAuCl$_4$ (aq) solution for 10 min, rinsed with water, and then dried with a stream of nitrogen gas. The sample was then loaded into a benchtop plasma cleaner (Harrick PDC 32G, 18 W) and exposed to an oxygen plasma at 0.8 Torr for 10 min to obtain the corresponding Au nanopatterns on the Si/SiO$_x$ surface. To ensure complete removal of polymer residues, the sample was then exposed to another 2 min of H$_2$/Ar plasma at 1.5 Torr.

Other BCPs were not solvent annealed with THF as they showed no improvement in hexagonal order as compared to "as spin-coated". All other procedures were identical to those described here for PS-*b*-P2VP (125 k-*b*-58.5 k).

Preparation of Plasmonic Stamp. The preparation of plasmonic stamps was based upon a process previously published by our group the preparation of catalytic Pd/Pt stamps,[58−60] with slight modifications. Briefly, the Au-nanopatterned Si/SiO$_x$ sample was placed in a desiccator with reduced pressure (1 Torr), together with an uncapped vial containing 15 μL of trichloro-(1H,1H,2H,2H-perfluorooctyl)silane for 60 min. The sample was then rinsed with ethanol and dried with a stream of nitrogen gas. To prepare the plasmonic stamp, h-PDMS (VDT-731, HMS 301, 2,4,6,8-tetramethyl-2,4,6,8-tetravinylcyclotetrasiloxane, and SIP6831.2) and 184 PDMS (degassed by centrifuging the PDMS prepolymer in a sealed tube at 3000 rpm for 30 min) were coated, in sequence, on the wafer surface in a Teflon mold, as per the photographs in Figure S1d (Supporting Information). Two curing steps (30 min for h-PDMS; and overnight for 184 PDMS) were performed at 65 °C in a vacuum oven after each PDMS coating step. After the curing steps, the plasmonic stamp was peeled off carefully from Si/SiO$_x$ substrate, soaked in hexane using a Soxhlet extractor for at least 6 h, rinsed with ethanol/water, and stored under vacuum prior to use.

Plasmonic Stamping on Hydride Terminated Si(111) Surface. Hydride-terminated Si(111) simples were obtained by immersing the RCA-processed Si(111) wafers in degassed 40% NH$_4$F(aq) for 5 min, immersed in deoxygenized water for 10 s, and dried with a stream of argon. In a nitrogen-filled glovebox, a hydride-terminated wafer was placed on a clean glass slip, and then neat alkene (30 μL) was carefully dropped from a microliter syringe on the hydride-terminated Si(111) surface. The plasmonic stamp was applied on the surface, and another glass slip cover was placed on top of the stamp. To apply reproducible pressure, two paper clamps were applied on both sides to fix the sandwich

structure, as shown in the photograph in Figure S2d (Supporting Information). White light from a 300 W ELH bulb was focused through a PCX lens, filtered by band-pass filters (CW526 or CW440), and shone on the sandwiched sample for 60 min with the intensity of 50 mW/cm^2 for the CW526 filter and 40 mW/cm^2 for CW440 filter. After the stamping steps, the wafer was rinsed thoroughly with dichloromethane and dried with a stream of argon gas prior to further analysis.

Thiol−Ene Chemistry and Gold Nanoparticle Binding. Citrate-capped gold nanoparticles were fabricated *via* a seed-mediated growth method following a procedure described elsewhere.[81] The procedure of visualization of a alkyl-patterned Si(111)−H substrate with gold nanoparticles closely follows the method previously described[58] and was slightly modified here. Briefly, a hydride-terminated Si(111) wafer was first stamped with 1,7-octadiene to form a pattern with terminal alkene groups. The sample was then immersed in concentrated KOH (4 mol/L) for 30 s and soaked overnight in oxygen-saturated water to remove all remaining Si−H$_x$ groups. The alkene-terminated patterned regions then underwent a thiol−ene reaction by immersing the sample in 0.1 mL of neat 1,4-butanedithiol, with illumination of ultraviolet visible light (254 nm, UVP pen lamp, Model 11SC-1) for 30 min, followed by rinsing with dichloromethane. Lastly, the thiol-patterned sample was immersed in a colloidal solution containing 10 nm citrate-capped Au nanoparticle for 3 h and then rinsed with toluene and dried with a stream of nitrogen gas.

Conflict of Interest: The authors declare no competing financial interest.

Supporting Information Available: AFM and SEM images for control experiments, photographs of experimental setups, contact angle statistics, and temperature measurements. This material is available free of charge *via* the Internet at http://pubs.acs.org.

REFERENCES AND NOTES

1. Qin, D.; Xia, Y.; Whitesides, G. M. Soft Lithography for Micro- and Nanoscale Patterning. *Nat. Protoc.* **2010**, *5*, 491−502.
2. Sreenivasan, S. V. Nanoscale Manufacturing Enabled by Imprint Lithography. *MRS Bull.* **2008**, *33*, 854−863.
3. Galatsis, K.; Wang, K. L.; Ozkan, M.; Ozkan, C. S.; Huang, Y.; Chang, J. P.; Monbouquette, H. G.; Chen, Y.; Nealey, P.; Botros, Y. Patterning and Templating for Nanoelectronics. *Adv. Mater.* **2010**, *22*, 769−778.
4. Kim, D. H.; Lee, H.; Lee, Y. K.; Nam, J. M.; Levchenko, A. Biomimetic Nanopatterns as Enabling Tools for Analysis and Control of Live Cells. *Adv. Mater.* **2010**, *22*, 4551−4566.
5. Lohmueller, T.; Aydin, D.; Schwieder, M.; Morhard, C.; Louban, I.; Pacholski, C.; Spatz, J. P. Nanopatterning by Block Copolymer Micelle Nanolithography and Bio-inspired Applications. *Biointerphases* **2011**, *6*, MR1−MR12.
6. Hakim, M. M. A.; Lombardini, M.; Sun, K.; Giustiniano, F.; Roach, P. L.; Davies, D. E.; Howarth, P. H.; de Planque, M. R. R.; Morgan, H.; Ashburn, P. Thin Film Polycrystalline Silicon Nanowire Biosensors. *Nano Lett.* **2012**, *12*, 1868−1872.
7. Trompoukis, C.; El Daif, O.; Depauw, V.; Gordon, I.; Poortmans, J. Photonic Assisted Light Trapping Integrated in Ultrathin Crystalline Silicon Solar Cells by Nanoimprint Lithography. *Appl. Phys. Lett.* **2012**, *101*, 103901.
8. Hong, S. H.; Zhu, J.; Mirkin, C. A. Multiple Ink Nanolithography: Toward a Multiple-Pen Nano-Plotter. *Science* **1999**, *286*, 523−525.
9. Gates, B. D.; Xu, Q. B.; Stewart, M.; Ryan, D.; Willson, C. G.; Whitesides, G. M. New Approaches to Nanofabrication: Molding, Printing, and Other Techniques. *Chem. Rev.* **2005**, *105*, 1171−1196.
10. Gong, J.; Lipomi, D. J.; Deng, J.; Nie, Z.; Chen, X.; Randall, N. X.; Nair, R.; Whitesides, G. M. Micro- and Nanopatterning

of Inorganic and Polymeric Substrates by Indentation Lithography. *Nano Lett.* **2010**, *10*, 2702–2708.

11. Shukla, S.; Vidal, X.; Furlani, E. P.; Swihart, M. T.; Kim, K.-T.; Yoon, Y.-K.; Urbas, A.; Prasad, P. N. Subwavelength Direct Laser Patterning of Conductive Gold Nanostructures by Simultaneous Photopolymerization and Photoreduction. *ACS Nano* **2011**, *5*, 1947–1957.

12. Kim, S. O.; Solak, H. H.; Stoykovich, M. P.; Ferrier, N. J.; de Pablo, J. J.; Nealey, P. F. Epitaxial Self-Assembly of Block Copolymers on Lithographically Defined Nanopatterned Substrates. *Nature* **2003**, *424*, 411–414.

13. Stoykovich, M. P.; Muller, M.; Kim, S. O.; Solak, H. H.; Edwards, E. W.; de Pablo, J. J.; Nealey, P. F. Directed Assembly of Block Copolymer Blends into Nonregular Device-Oriented Structures. *Science* **2005**, *308*, 1442–1446.

14. Mann, S. Self-Assembly and Transformation of Hybrid Nano-Objects and Nanostructures under Equilibrium and Non-Equilibrium Conditions. *Nat. Mater.* **2009**, *8*, 781–792.

15. *International Technology Roadmap for Semiconductors*, 2013 ed.; Semiconductor Industry Association: San Jose, CA, 2013.

16. Bates, C. M.; Maher, M. J.; Janes, D. W.; Ellison, C. J.; Willson, C. G. Block Copolymer Lithography. *Macromolecules* **2014**, *47*, 2–12.

17. Shin, D. O.; Mun, J. H.; Hwang, G.-T.; Yoon, J. M.; Kim, J. Y.; Yun, J. M.; Yang, Y.-B.; Oh, Y.; Lee, J. Y.; Shin, J.; et al. Multicomponent Nanopatterns by Directed Block Copolymer Self-Assembly. *ACS Nano* **2013**, *7*, 8899–8907.

18. Luo, M.; Epps, T. H., III Directed Block Copolymer Thin Film Self-Assembly: Emerging Trends in Nanopattern Fabrication. *Macromolecules* **2013**, *46*, 7567–7579.

19. Ross, C. A.; Berggren, K. K.; Cheng, J. Y.; Jung, Y. S.; Chang, J.-B. Three-Dimensional Nanofabrication by Block Copolymer Self-Assembly. *Adv. Mater.* **2014**, *26*, 4386–4396.

20. Lohmueller, T.; Bock, E.; Spatz, J. P. Synthesis of Quasi-Hexagonal Ordered Arrays of Metallic Nanoparticles with Tuneable Particle Size. *Adv. Mater.* **2008**, *20*, 2297–2302.

21. Aizawa, M.; Buriak, J. M. Block Copolymer Templated Chemistry for the Formation of Metallic Nanoparticle Arrays on Semiconductor Surfaces. *Chem. Mater.* **2007**, *19*, 5090–5101.

22. Liu, C.-C.; Ramirez-Hernandez, A.; Han, E.; Craig, G. S. W.; Tada, Y.; Yoshida, H.; Kang, H.; Ji, S.; Gopalan, P.; de Pablo, J. J.; et al. Chemical Patterns for Directed Self-Assembly of Lamellae-Forming Block Copolymers with Density Multiplication of Features. *Macromolecules* **2013**, *46*, 1415–1424.

23. Jung, H.; Hwang, D.; Kim, E.; Kim, B. J.; Lee, W. B.; Poelma, J. E.; Kim, J.; Hawker, C. J.; Huh, J.; Ryu, D. Y.; et al. Three-Dimensional Multilayered Nanostructures with Controlled Orientation of Microdomains from Cross-Linkable Block Copolymers. *ACS Nano* **2011**, *5*, 6164–6173.

24. Gu, W. Y.; Zhao, H.; Wei, Q. S.; Coughlin, E. B.; Theato, P.; Russell, T. P. Line Patterns from Cylinder-Forming Photocleavable Block Copolymers. *Adv. Mater.* **2013**, *25*, 4690–4695.

25. Wu, N. L. Y.; Zhang, X.; Murphy, J. N.; Chai, J.; Harris, K. D.; Buriak, J. M. Density Doubling of Block Copolymer Templated Features. *Nano Lett.* **2012**, *12*, 264–268.

26. Jin, C.; Murphy, J. N.; Harris, K. D.; Buriak, J. M. Deconvoluting the Mechanism of Microwave Annealing of Block Copolymer Thin Films. *ACS Nano* **2014**, *8*, 3979–3991.

27. Zhang, X.; Murphy, J. N.; Wu, N. L.; Harris, K. D.; Buriak, J. M. Rapid Assembly of Nanolines with Precisely Controlled Spacing from Binary Blends of Block Copolymers. *Macromolecules* **2011**, *44*, 9752–9757.

28. Chai, J.; Wang, D.; Fan, X.; Buriak, J. M. Assembly of Aligned Linear Metallic Patterns on Silicon. *Nat. Nanotechnol.* **2007**, *2*, 500–506.

29. Stoykovich, M. P.; Kang, H.; Daoulas, K. C.; Liu, G.; Liu, C.-C.; de Pablo, J. J.; Mueller, M.; Nealey, P. F. Directed Self-Assembly of Block Copolymers for Nanolithography: Fabrication of Isolated Features and Essential Integrated Circuit Geometries. *ACS Nano* **2007**, *1*, 168–175.

30. Tavakkoli, K. G. A.; Gotrik, K. W.; Hannon, A. F.; Alexander-Katz, A.; Ross, C. A.; Berggren, K. K. Templating Three-Dimensional Self-Assembled Structures in Bilayer Block Copolymer Films. *Science* **2012**, *336*, 1294–1298.

31. Bosworth, J. K.; Paik, M. Y.; Ruiz, R.; Schwartz, E. L.; Huang, J. Q.; Ko, A. W.; Smilgies, D.-M.; Black, C. T.; Ober, C. K. Control of Self-Assembly of Lithographically Patternable Block Copolymer Films. *ACS Nano* **2008**, *2*, 1396–1402.

32. Black, C. T.; Ruiz, R.; Breyta, G.; Cheng, J. Y.; Colburn, M. E.; Guarini, K. W.; Kim, H. C.; Zhang, Y. Polymer Self Assembly in Semiconductor Microelectronics. *IBM J. Res. Dev.* **2007**, *51*, 605–633.

33. He, C.; Stoykovich, M. P. Profile Control in Block Copolymer Nanostructures Using Bilayer Thin Films for Enhanced Pattern Transfer Processes. *Adv. Funct. Mater.* **2014**, *24*, 7078–7084.

34. Spatz, J. P.; Herzog, T.; Mossmer, S.; Ziemann, P.; Möller, M. Micellar Inorganic-Polymer Hybrid Systems - a Tool for Nanolithography. *Adv. Mater.* **1999**, *11*, 149–153.

35. Chai, J.; Buriak, J. M. Using Cylindrical Domains of Block Copolymers to Self-Assemble and Align Metallic Nanowires. *ACS Nano* **2008**, *2*, 489–501.

36. Jung, Y. S.; Ross, C. A. Solvent-Vapor-Induced Tunability of Self-Assembled Block Copolymer Patterns. *Adv. Mater.* **2009**, *21*, 2540–2545.

37. Gu, X.; Liu, Z.; Gunkel, I.; Chourou, S.; Hong, S. W.; Olynick, D. L.; Russell, T. P. High Aspect Ratio Sub-15 nm Silicon Trenches from Block Copolymer Templates. *Adv. Mater.* **2012**, *24*, 5688–5694.

38. Black, C. Self-Aligned Self Assembly of Multi-Nanowire Silicon Field Effect Transistors. *Appl. Phys. Lett.* **2005**, *87*, 163116.

39. Huang, Y. G.; Kim, T. W.; Long, S. S.; Mawst, L. J.; Kuech, T. F.; Nealey, P. F.; Dai, Y. S.; Wang, Z. H.; Guo, W.; Forbes, D.; et al. InAs Nanowires Grown by Metal-Organic Vapor-Phase Epitaxy (MOVPE) Employing PS/PMMA Diblock Copolymer Nanopatterning. *Nano Lett.* **2013**, *13*, 5979–5984.

40. Kuech, T. F.; Mawst, L. J. Nanofabrication of III−V Semiconductors Employing Diblock Copolymer Lithography. *J. Phys. D: Appl. Phys.* **2010**, *43*, 183001.

41. Ji, S.; Liu, C.-C.; Liu, G.; Nealey, P. F. Molecular Transfer Printing Using Block Copolymers. *ACS Nano* **2010**, *4*, 599–609.

42. Deng, X.; Buriak, J. M.; Dai, P.-X.; Wan, L.-J.; Wang, D. Block Copolymer-Templated Chemical Nanopatterning on Pyrolyzed Photoresist Carbon Films. *Chem. Commun.* **2012**, *48*, 9741–9743.

43. Linic, S.; Christopher, P.; Ingram, D. B. Plasmonic-Metal Nanostructures for Efficient Conversion of Solar to Chemical Energy. *Nat. Mater.* **2011**, *10*, 911–921.

44. Sharma, B.; Cardinal, M. F.; Kleinman, S. L.; Greeneltch, N. G.; Frontiera, R. R.; Blaber, M. G.; Schatz, G. C.; Van Duyne, R. P. High-Performance SERS Substrates: Advances and Challenges. *MRS Bull.* **2013**, *38*, 615–624.

45. Liu, Z.; Hou, W.; Pavaskar, P.; Aykol, M.; Cronin, S. B. Plasmon Resonant Enhancement of Photocatalytic Water Splitting under Visible Illumination. *Nano Lett.* **2011**, *11*, 1111–1116.

46. Choi, H.; Chen, W. T.; Kamat, P. V. Know Thy Nano Neighbor. Plasmonic Versus Electron Charging Effects of Metal Nanoparticles in Dye-Sensitized Solar Cells. *ACS Nano* **2012**, *6*, 4418–4427.

47. Atwater, H. A.; Polman, A. Plasmonics for Improved Photovoltaic Devices. *Nat. Mater.* **2010**, *9*, 205–213.

48. Sugimura, H.; Mo, S.; Yamashiro, K.; Ichii, T.; Murase, K. Photochemical Assembly of Gold Nanoparticle Arrays Covalently Attached to Silicon Surface Assisted by Localized Plasmon in the Nanoparticles. *J. Phys. Chem. C* **2013**, *117*, 2480–2485.

49. Linford, M. R.; Chidsey, C. E. D. Alkyl Monolayers Covalently Bonded to Silicon Surfaces. *J. Am. Chem. Soc.* **1993**, *115*, 12631–12632.

50. Chatgilialoglu, C. Structural and Chemical-Properties of Silyl Radicals. *Chem. Rev.* **1995**, *95*, 1229–1251.

51. Wang, X.; Ruther, R. E.; Streifer, J. A.; Hamers, R. J. UV-Induced Grafting of Alkenes to Silicon Surfaces:

Photoemission Versus Excitons. *J. Am. Chem. Soc.* **2010**, *132*, 4048–4049.

52. Gooding, J. J.; Ciampi, S. The Molecular Level Modification of Surfaces: From Self-Assembled Monolayers to Complex Molecular Assemblies. *Chem. Soc. Rev.* **2011**, *40*, 2704–2718.

53. Stewart, M. P.; Buriak, J. M. Exciton-Mediated Hydrosilylation on Photoluminescent Nanocrystalline Silicon. *J. Am. Chem. Soc.* **2001**, *123*, 7821–7830.

54. Wong, K. T.; Lewis, N. S. What a Difference a Bond Makes: The Structural, Chemical, and Physical Properties of Methyl-Terminated Si(111) Surfaces. *Acc. Chem. Res.* **2014**, *47*, 3037–3044.

55. Buriak, J. M. Organometallic Chemistry on Silicon and Germanium Surfaces. *Chem. Rev.* **2002**, *102*, 1271–1308.

56. Michalak, D. J.; Amy, S. R.; Aureau, D.; Dai, M.; Estève, A.; Chabal, Y. J. Nanopatterning Si (111) Surfaces as a Selective Surface-Chemistry Route. *Nat. Mater.* **2010**, *9*, 266–271.

57. Buriak, J. M. Illuminating Silicon Surface Hydrosilylation: An Unexpected Plurality of Mechanisms. *Chem. Mater.* **2014**, *26*, 763–772.

58. Mizuno, H.; Buriak, J. M. Catalytic Stamp Lithography for Sub-100 nm Patterning of Organic Monolayers. *J. Am. Chem. Soc.* **2008**, *130*, 17656–17657.

59. Mizuno, H.; Buriak, J. M. Nanoscale Patterning of Organic Monolayers by Catalytic Stamp Lithography: Scope and Limitations. *ACS Appl. Mater. Interfaces* **2009**, *1*, 2711–2720.

60. Mizuno, H.; Buriak, J. M. Building Upon Patterned Organic Mono Layers Produced *via* Catalytic Stamp Lithography. *ACS Appl. Mater. Interfaces* **2010**, *2*, 2301–2307.

61. Li, Y.-H.; Wang, D.; Buriak, J. M. Molecular Layer Deposition of Thiol- Ene Multilayers on Semiconductor Surfaces. *Langmuir* **2009**, *26*, 1232–1238.

62. Peng, H.; Wang, C.; Xi, W.; Kowalski, B. A.; Gong, T.; Xie, X.; Wang, W.; Nair, D. P.; McLeod, R. R.; Bowman, C. N. Facile Image Patterning *via* Sequential Thiol-Michael/Thiol-Yne Click Reactions. *Chem. Mater.* **2014**, *26*, 6819–6826.

63. Strohmeier, B. R. Copper/Silver/Gold Alloy by XPS. *Surf. Sci. Spectra* **1994**, *3*, 175–181.

64. Louette, P.; Bodino, F.; Pireaux, J.-J. Poly (Dimethyl Siloxane)(PDMS) XPS Reference Core Level and Energy Loss Spectra. *Surf. Sci. Spectra* **2005**, *12*, 38–43.

65. Brongersma, M. L.; Halas, N. J.; Nordlander, P. Plasmon-Induced Hot Carrier Science and Technology. *Nat. Nanotechnol.* **2015**, *10*, 25–34.

66. Baek, S.-W.; Noh, J.; Lee, C.-H.; Kim, B.; Seo, M.-K.; Lee, J.-Y. Plasmonic Forward Scattering Effect in Organic Solar Cells: A Powerful Optical Engineering Method. *Sci. Rep.* **2013**, *3*, 1726.

67. Jain, P. K.; Lee, K. S.; El-Sayed, I. H.; El-Sayed, M. A. Calculated Absorption and Scattering Properties of Gold Nanoparticles of Different Size, Shape, and Composition: Applications in Biological Imaging and Biomedicine. *J. Phys. Chem. B* **2006**, *110*, 7238–7248.

68. Neumann, O.; Urban, A. S.; Day, J.; Lal, S.; Nordlander, P.; Halas, N. J. Solar Vapor Generation Enabled by Nanoparticles. *ACS Nano* **2013**, *7*, 42–49.

69. Qiu, J.; Wei, W. D. Surface Plasmon-Mediated Photothermal Chemistry. *J. Phys. Chem. C* **2014**, *118*, 20735–20749.

70. Bateman, J. E.; Eagling, R. D.; Worrall, D. R.; Horrocks, B. R.; Houlton, A. Alkylation of Porous Silicon by Direct Reaction with Alkenes and Alkynes. *Angew. Chem., Int. Ed.* **1998**, *37*, 2683–2685.

71. Govorov, A. O.; Richardson, H. H. Generating Heat with Metal Nanoparticles. *Nano Today* **2007**, *2*, 30–38.

72. Hogan, N. J.; Urban, A. S.; Ayala-Orozco, C.; Pimpinelli, A.; Nordlander, P.; Halas, N. J. Nanoparticles Heat through Light Localization. *Nano Lett.* **2014**, *14*, 4640–4645.

73. Baffou, G.; Berto, P.; Urena, E. B.; Quidant, R.; Monneret, S.; Polleux, J.; Rigneault, H. Photoinduced Heating of Nanoparticle Arrays. *ACS Nano* **2013**, *7*, 6478–6488.

74. Mukherjee, S.; Libisch, F.; Large, N.; Neumann, O.; Brown, L. V.; Cheng, J.; Lassiter, J. B.; Carter, E. A.; Nordlander, P.; Halas, N. J. Hot Electrons Do the Impossible: Plasmon-Induced Dissociation of H_2 on Au. *Nano Lett.* **2012**, *13*, 240–247.

75. Gomes Silva, C.; Juárez, R.; Marino, T.; Molinari, R.; García, H. Influence of Excitation Wavelength (UV or Visible Light) on the Photocatalytic Activity of Titania Containing Gold Nanoparticles for the Generation of Hydrogen or Oxygen from Water. *J. Am. Chem. Soc.* **2010**, *133*, 595–602.

76. Tian, Y.; Tatsuma, T. Mechanisms and Applications of Plasmon-Induced Charge Separation at TiO_2 Films Loaded with Gold Nanoparticles. *J. Am. Chem. Soc.* **2005**, *127*, 7632–7637.

77. Huck, L. A.; Buriak, J. M. Toward a Mechanistic Understanding of Exciton-Mediated Hydrosilylation on Nanocrystalline Silicon. *J. Am. Chem. Soc.* **2012**, *134*, 489–497.

78. Sundararaman, R.; Narang, P.; Jermyn, A. S.; Goddard, W. A., III; Atwater, H. A. Theoretical Predictions for Hot-Carrier Generation from Surface Plasmon Decay. *Nat. Commun.* **2014**, *5*, 5788.

79. Anger, P.; Bharadwaj, P.; Novotny, L. Enhancement and Quenching of Single-Molecule Fluorescence. *Phys. Rev. Lett.* **2006**, *96*, 113002.

80. Lee, J.; Javed, T.; Skeini, T.; Govorov, A. O.; Bryant, G. W.; Kotov, N. A. Bioconjugated Ag Nanoparticles and Cdte Nanowires: Metamaterials with Field-Enhanced Light Absorption. *Angew. Chem., Int. Ed.* **2006**, *45*, 4819–4823.

81. Jana, N. R.; Gearheart, L.; Murphy, C. J. Seeding Growth for Size Control of 5−40 nm Diameter Gold Nanoparticles. *Langmuir* **2001**, *17*, 6782–6786.